Combining fluorescence fluctuations and photobleaching to quantify surface density

Julius Sefkow-Werner, Elisa Migliorini, Catherine Picart, Dwiria Wahyuni, Irène Wang, Antoine Delon

Combining fluorescence fluctuations and photobleaching to quantify surface density

Journal:	*Analytical Chemistry*
Manuscript ID	ac-2021-05513t.R2
Manuscript Type:	Article
Date Submitted by the Author:	n/a
Complete List of Authors:	Sefkow-Werner, Julius; CNRS Delegation Rhone-Auvergne; UMR5628 MIGLIORINI, Elisa; CNRS Delegation Rhone-Auvergne; UMR5628 Picart, Catherine; CNRS Delegation Rhone-Auvergne; UMR5628 wahyuni, dwiria; Universitas Tanjungpura, Department of Physics Wang, Irene; Université Grenoble Alpes, LIPhy DELON, Antoine; Universite Grenoble Alpes, LIPhy

Combining fluorescence fluctuations and photobleaching to quantify surface density

Julius Sefkow-Werner,[†,‡] Elisa Migliorini,[*,†,‡] Catherine Picart,[†,‡] Dwiria Wahyuni,[¶,§] Irène Wang,[¶] and Antoine Delon[*,¶]

† *Univ. Grenoble Alpes, INSERM U1292, CEA, CNRS EMR 5000 BRM, IRIG Institute, CEA, 38054 Grenoble, France*

‡ *Grenoble Institute of Engineering, CNRS UMR 5628, LMGP, 38016 Grenoble, France*

¶ *Univ. Grenoble Alpes, CNRS, LIPhy, 38000 Grenoble, France*

§ *Current address: Department of Physics, Universitas Tanjungpura, Pontianak 78124, Indonesia*

E-mail: elisa.migliorini@cea.fr; antoine.delon@univ-grenoble-alpes.fr

Abstract

We have established a self-calibrated method, called *pbFFS* for *photobleaching fluctuation fluorescence spectroscopy*, which aims to characterize molecules or particles labeled with an unknown distribution of fluorophores. Using photobleaching as a control parameter, pbFFS provides information on the distribution of fluorescent labels and a reliable estimation of the absolute density or concentration of these molecules. We present a complete theoretical derivation of the pbFFS approach and experimentally apply it to measure the surface density of a monolayer of fluorescently tagged streptavidin molecules, which can be used as a base platform for biomimetic systems. The surface density measured by pbFFS is consistent with the results of spectroscopic ellipsometry, a standard surface technique. However, pbFFS has two main advantages:

it enables *in situ* characterization (no dedicated substrates are required) and can be applied to low masses of adsorbed molecules, which we demonstrate here by quantifying the density of biotin-Atto molecules that bind to the streptavidin layer. In addition to molecules immobilized on a surface, we also applied pbFFS to molecules diffusing in solution, to confirm the distribution of fluorescent labels found on a surface. Hence, pbFFS provides a set of tools for investigating molecules labeled with a variable number of fluorophores, with the aim of quantifying either the number of molecules or the distribution of fluorescent labels, the latter case being especially relevant for oligomerization studies.

Introduction

Biomimetic approaches are popular in medical applications and cellular studies. As the extracellular matrix (ECM) plays a complex role in cell responses to drugs, growth factors, and morphological cues,[1] it is advantageous to design biomaterials mimicking the natural environment of cells in the body in order to enhance the efficiency of biomedical products. Moreover, these biomaterials can bring a deeper understanding of the influence of selected components of the ECM on cellular processes such as proliferation, migration, and differentiation.[2] Developing these platforms requires precise control of the immobilized compounds. Standard surface techniques include spectroscopic ellipsometry and quartz crystal microbalance with dissipation (QCM-D) monitoring.[3,4] However, these techniques are *ex situ*, as the platforms must be built on auxiliary substrates, which may affect the functionalization process. Moreover, low masses of adsorbed molecules cannot be detected by the above techniques. Fluorescence-based methods would, in principle, enable both *in situ* characterization (i.e., with substrates used for cellular studies) and the detection of adsorbed molecules at low surface densities.

Based on fluorescently labeled molecules, a simple image provides relative information on molecular density through its intensity, but estimating the absolute value of the number of

molecules requires additional sensitive calibrations.[5] Alternative approaches based on single-molecule strategies have been reported, but have been adapted only for very low surface densities.[6] In contrast, fluorescence fluctuation spectroscopy (FFS) techniques[7] and, more specifically, image correlation spectroscopy (ICS), which is suited to the characterization of immobile molecules, are intended for absolute quantification. Historically, these methods have arisen from fluorescence correlation spectroscopy (FCS) and are based on the notion that a signal originating from a submicrometer region within a sample, corresponding to the point spread function (PSF) of the microscope, exhibits statistical fluctuations, as this PSF region does not always include the same number of molecules. The relative amplitude of these fluctuations provides an estimation of the average number of molecules in the PSF region and hence the concentration or density. Molecules cross the PSF either by spontaneous motion, as in the case of FCS, or by scanning of an excitation laser (similar to confocal microscopy), as in the case of ICS. ICS has been used to assess oligomerization[8] and to qualitatively detect the presence of aggregates through an increase in brightness or a corresponding decrease in number density.[9,10]

Standard FFS techniques can only provide reliable quantitative information if all molecules have the same brightness (or if the distribution of brightness is known). Yet, commercially available large proteins are rarely all labeled with the same number of fluorophores; thus, they present a distribution of brightness. In this case, the number density of fluorescent entities (molecules or particles) estimated by conventional FFS is underestimated: indeed, part of the measured fluctuations arises from variations in brightness rather than variations in the number of entities, as is usually assumed in FFS. More precisely, if the brightness distribution is characterized by a mean value, $\bar{\epsilon}$, and a standard deviation (SD), σ_ϵ, it can be shown (following[9,11]) that the mean number of entities in the PSF volume or area, as measured by FFS, is related to the true number of entities, N, by:

$$N_{FFS} = \frac{N}{1 + (\sigma_\epsilon/\bar{\epsilon})^2} \tag{1}$$

Consequently, a wider brightness distribution corresponds to a more pronounced underestimation of the number density. The same bias affects the estimation of average brightness (which tends to be overestimated). Using only standard FFS methods, there is no way to evaluate this bias.

The present work aims to apply photobleaching as a control parameter to accurately measure the density of surfaces coated with multi-labeled entities. The combination of FFS and photobleaching has been previously proposed and used to estimate the degree of fluorescent labeling,[12] the size of oligomers,[13,14] and the surface density of molecules.[15] However, thus far, practical implementations have either been limited to the specific case of a Poisson distribution of brightness[12,15] or failed to decipher the real parameters that could be deduced from photobleaching decay.[13,14] We present here a complete theoretical description of a method combining FFS and photobleaching, termed *pbFFS* for *photobleaching FFS*. Compared with previous works, our derivation remains valid regardless of the distribution of fluorescent labels. More precisely, we show that the measured brightness always decays linearly with photobleaching. Hence, exactly two outputs can be extracted from this decay: (i) the brightness of a single fluorescent label and (ii) a factor depending on the mean and variance of the number of fluorescent labels per entity. We stress the fact that the presented method has the advantage of being *calibration-free*.

The pbFFS method is experimentally validated on substrates covered with monolayers of streptavidin (SAv) molecules via a linker, used as a platform to build biomimetic surfaces step-by-step by adsorbing biotinylated molecules on top of it.[3,16] Using Alexa-tagged molecules (SAv-Alex), we estimated the absolute number density of SAv molecules covering the substrate, which agrees with independent spectroscopic ellipsometry measurements. We show that pbFFS is capable of measuring SAv-Alex surface densities that span over two orders of magnitude. pbFFS was also used to quantify the number of biotinylated fluorescent molecules (Atto-labeled biotin, bAtto) attached to a SAv base layer. In this case, the mass of adsorbed molecules was too low to be accurately measured by QCM-D or ellipsometry

(because the mass of bAtto is only 1 kDa compared with the mass of SAv at 55 kDa). Interestingly, by performing control photobleaching-FCS experiments, we also found that bAtto molecules are prone to aggregation in solution, which potentially impacts the manner in which they bind to the SAv base layer.

Principles of pbFFS

As illustrated in Fig. 1A and D, a pbFFS experiment consists of alternating photobleaching phases, where a high laser power is applied to the sample to bleach a fraction of the fluorescent labels (e.g., Alexa) borne by the entities (e.g., SAv), and measurement phases at a reduced laser power. During the latter phase, the fluorescence signal F, the mean number of entities N_{FFS}, and the brightness, defined as $B_{FFS} = F/N_{FFS}$, are measured. As more fluorescent labels are photobleached, the image intensity (in ICS, Fig. 1B) or the photon count rate (in FCS, Fig. 1C) decreases, while the autocorrelation amplitude increases, denoting a reduction in the number of entities N_{FFS} in the PSF submicrometer region.

We consider a sample consisting of entities labeled with multiple fluorophores of identical brightness, ϵ. The distribution of the number of these labels per entity before photobleaching is characterized by the mean and SD, given as m and σ, respectively. It can be shown (see Section S1 of the Supporting Information (SI)) that the measured brightness B_{FFS} is an affine function of the photobleaching stage p, defined as the fluorescence signal normalized by its initial value, i.e., $p = F/F(1)$:

$$B_{FFS}(p) = \epsilon(1 + S_{\sigma m}p) \tag{2}$$

where $S_{\sigma m}$ is the slope normalized by the single label brightness. This slope is related to the SD and mean value of the distribution according to:

$$S_{\sigma m} = \sigma^2/m + m - 1 \tag{3}$$

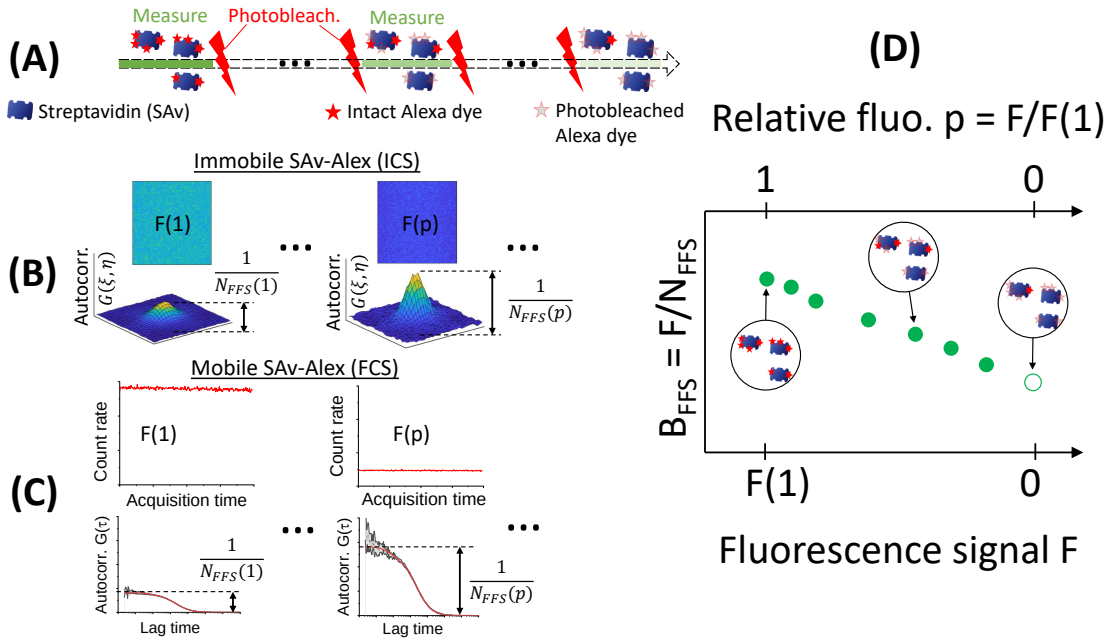

Figure 1: Principle of a pbFFS experiment exemplified by SAv molecules labeled with Alexa dye (SAv-Alex). (A) Experiment timeline showing the alternation of measurement phases (green sections) and photobleaching phases (red flashes). After each photobleaching period, the number of intact Alexa labels is reduced, and thus, the SAv-Alex molecules become less bright. (B) Images of immobilized SAv-Alex (top row) and corresponding spatial autocorrelation $G(\xi, \eta)$ (bottom row), as measured by ICS during the course of an experiment. The mean fluorescence F decreases, whereas the autocorrelation amplitude increases (denoting a decrease in the number of SAv-Alex molecules N_{FFS}) as photobleaching advances. (C) Detected count rate (top row) and corresponding temporal autocorrelation $G(\tau)$ (bottom row) measured for solutions of mobile SAv-Alex molecules by FCS. As in ICS, when the sample is photobleached, both the mean count rate F and the number of SAv-Alex molecules N_{FFS} decrease. (D) Measured brightness ($B_{FFS} = F/N_{FFS}$) *versus* fluorescence signal during photobleaching. The brightness of the SAv-Alex molecules tends toward that of single Alexa labels as the fluorescence signal vanishes. Note that the photobleaching stage can be parameterized by the relative fluorescence p defined as the ratio of the fluorescence signal to its initial value.

The true total number of entities is then given by:

$$N = F(1)/m\epsilon \tag{4}$$

The linear decay of the measured brightness *versus* the fluorescence signal is valid for any distribution of fluorescent labels, assuming that all fluorescent labels have the same brightness

ϵ and a constant probability of bleaching regardless of the number per entity. A straightforward result of any pbFFS experiment is the single label brightness, ϵ. This is an interesting output because one can derive the total number of fluorescent labels, $Nm = F(1)/\epsilon$, using Eq. 4. Exploiting the slope, $S_{\sigma m}$, is more complex because, in the general case, it is impossible to independently determine the mean value, m, and the SD, σ, of the number of fluorescent labels per entity, as shown by Eq. 3. However, specific fluorescent label distributions add constraints such that, in practice, the m values are reduced to a given range (for details, see Section S2 in the SI). This case holds for the SAv monolayer, as discussed in the next section.

Implementation of the analysis method

Effect of the background

When performing pbFFS experiments, we sometimes observe, both on surfaces and in solution, photobleaching decays that do not exhibit a linear behavior (as the red line in Fig. 2A), but drop to lower values of brightness when the fluorescence signal becomes small (green curve). This behavior is due to an uncorrelated background, BG, that contributes to the detected signal, thus making the relative fluctuations smaller and consequently the apparent number of entities larger, which leads to a lower brightness, as described in.[17] Nevertheless, it is possible to incorporate the background as a free parameter in the photobleaching decay analysis by rewriting Eq. 2 as:

$$B_{FFS}(p) = \epsilon \left(1 - \frac{r_{BG}}{p}\right) \left(1 + S_{\sigma m} \frac{p - r_{BG}}{1 - r_{BG}}\right) \tag{5}$$

where $r_{BG} = BG/F(1)$ is the background normalized to the total initial signal (i.e., including the background itself). Correspondingly, p becomes the relative total signal, including the background. The latter originates either from light scattering (due to a glass

substrate or the walls of PDMS microwells, see SI) or from some bulk fluorescence that would not be properly filtered out by confocal detection. This effect appears to be especially pronounced and difficult to mitigate in solution. Thus, the fit of the photobleaching decay shown in Fig. 2A gives the parameters ϵ and $S_{\sigma m}$ (and BG, if relevant).

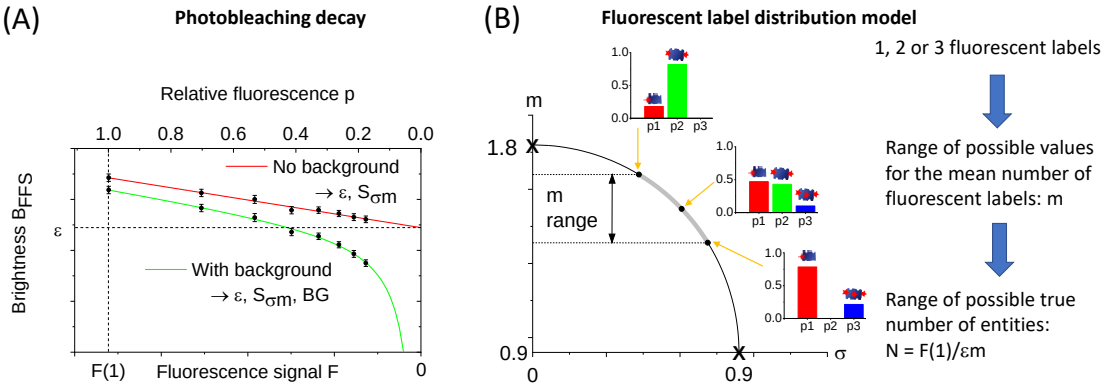

Figure 2: Schematic for implementing the brightness decay analysis. (A) Upon photobleaching, the brightness, B_{FFS}, decreases linearly *versus* the fluorescence signal, F or p (red solid line), thus providing the output parameters ϵ and $S_{\sigma m}$. For cases with background (green solid line), an additional parameter, BG, can be estimated by fitting the decay (see text for details). (B) By combining the relation between m and σ corresponding to the measured value of $S_{\sigma m}$ and the constraints derived from three non-zero probabilities (p_1, p_2, and p_3 for 1, 2, or 3 fluorescent labels), the possible m values are restricted to a limited range. Three examples of probability distributions corresponding to the minimum, maximum, and central values of m are depicted for $S_{\sigma m} = 0.8$. Finally, this analysis provides a value of the mean number of fluorescent labels, m, which, when combined with the initial fluorescence signal, $F(1)$ and the parameter ϵ, leads to an estimation of the true number of entities, N.

Accounting for the fluorescent label distribution

The manufacturer gives a value of 2 for the degree of fluorescent labeling of SAv-Alex; thus, we take this number as an approximate value and consider that each SAv protein can bear 1, 2, or 3 Alexa labels, with probabilities p_1, p_2, and p_3. The key point is that this discrete distribution of probabilities has only two independent degrees of freedom (once the probabilities p_1 and p_2 are known, the last probability, p_3, automatically follows). Additionally, we show in Section S1 in the SI that the σ and m values are constrained along a circle due to Eq. 3. Combined with the distribution properties, these constraints lead to a limited range

of possible mean numbers of fluorescent labels. In our current situation, it can be shown (see Section S2, Eq. S11-S15, and Fig. S1 in the SI) that if $S_{\sigma m} \leq 1$, then $\frac{3}{3-S_{\sigma m}} \leq m \leq \frac{2}{2-S_{\sigma m}}$, while if $1 < S_{\sigma m} \leq 2$, then $\frac{3}{3-S_{\sigma m}} \leq m \leq \frac{6}{4-S_{\sigma m}}$ (we never measured $S_{\sigma m} > 2$). Fig. 2B schematically shows a few examples of probability distributions (p_1, p_2, p_3) corresponding to the value $S_{\sigma m} = 0.8$ that is often found for SAv-Alex, ranging from the narrowest distribution (minimum value of σ) with the largest mean value, m, to the widest distribution with the smallest m value. Clearly, the latter distribution is unrealistic, as it would correspond to SAv proteins that never bear 2 fluorescent labels, while most of them bear 1 fluorescent label and some bear 3. It can be shown (see Section S2 in the SI) that the condition required for the probability of bearing 3 fluorescent labels to be smaller than that for 2 labels implies that $m > \frac{1}{1-\frac{3}{8}S_{\sigma m}}$.

Interestingly, if we had hypothesized that SAv proteins could bear 2, 3, or 4 Alexa labels, we would obtain either no solution when $S_{\sigma m} < 1$ or, for the few cases in which we measure $1 \leq S_{\sigma m} \leq 1.5$, a vast majority of SAv molecules bearing 2 Alexa labels and almost no molecules bearing 3 or 4 labels, which is consistent with the model retained throughout this work (see Section S2 and Eq. S16 in the SI).

For biotinylated fluorescent molecules, it is clear from the bAtto formula (given in the product specification) that these molecules correspond to one single Atto dye. However, as noted above, because a SAv protein in the base layer exposes 1 to 3 free biotin-binding sites, several bAtto molecules can colocalize on a single SAv protein. Therefore, we also assume that biotinylated entities can bear 1, 2, or 3 fluorescent labels.

To conclude, from our analysis of the brightness decay, we obtain a range of values for m and hence a range of values for the true number of fluorescent entities, $N = F(1)/m\epsilon$, which in turn leads to the final surface density given by $N/\pi {w_r}^2$.

Experimental results

SAv layers are densely packed

Photobleaching ICS experiments were performed on SAv layers with different percentages of fluorescently labeled SAv (SAv-Alex), including 1%, 10%, 50%, and 100%. Because ICS usually performs better for relatively low surface densities, these dilutions were utilized to examine the robustness of our method in a range of densities relevant for biomimetic surfaces. Details regarding the sample preparation, acquisition protocol, and data analysis are given in Section S4 in the SI.

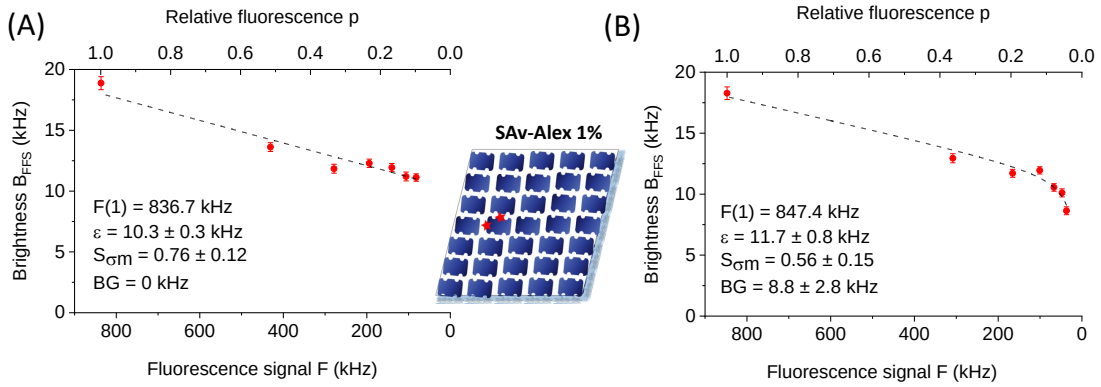

Figure 3: Characteristic brightness decay *versus* the fluorescence signal for a SAv layer prepared with a 1% dilution of SAv-Alex. (A) Example without background (i.e., fixed to 0), showing the linear decay and fit (dashed black line) with the ϵ and $S_{\sigma m}$ outputs corresponding to the measured (red) points. The errors bars are the standard errors of the mean calculated from 8×8 sub-images. (B) In the presence of background, the corresponding parameter, BG, can be fitted (representing approximately 1% of the initial fluorescence signal, $F(1)$), while the other outputs, ϵ and $S_{\sigma m}$, are consistent with the results of the background-free case.

Fig. 3A shows the characteristic brightness decay *versus* the fluorescence signal obtained for a 1% dilution of SAv-Alex. The parameters estimated from the fit, $\epsilon = 10.3$ kHz and $S_{\sigma m} = 0.76$, correspond to an initial brightness given by $B_{FFS}(1) = \epsilon(1 + S_{\sigma m})$, which is approximately 1.8 times larger than the single fluorescent label brightness. Consequently, if the distribution of the number of fluorescent labels per molecule was single-valued, one would be close to the situation of 2 Alexa dyes per SAv molecule, which corresponds to the

manufacturer specifications. However, using the theory presented in Section S2 in the SI, we can estimate the range of m values compatible with both the possible numbers of fluorescent labels and the estimated value of $S_{\sigma m}$ at $[1.40, 1.61]$ (see Section S2, Fig. S1, and Eq. S14 in the SI). This result corresponds to a surface density in the range of 316-363 molecules per μm^2 for fluorescently labeled SAv molecules at a 1% dilution (using w_r= 0.22 μm for this data set). Fig. 3B shows another result obtained with the same dilution of SAv-Alex, while exemplifying the effect of background on the brightness decay. Although the background accounts for only approximately 1% of the total initial signal, the deformation from linearity of the brightness decay is very pronounced at the end of the process. However, the decay can still be well fitted using one additional parameter, BG, while the other parameters remain consistent with the values estimated without a background.

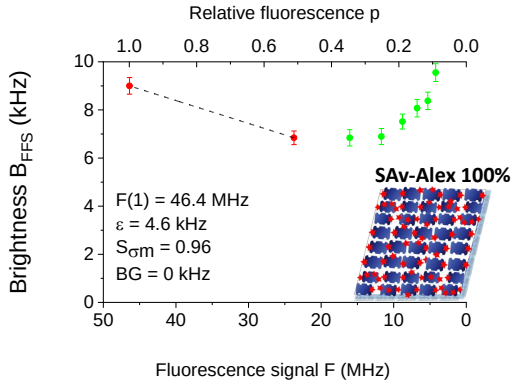

Figure 4: Example of the dramatic effect on the brightness decay caused by fluorescence quenching between Alexa555 fluorophores of a SAv layer prepared with 100% SAv-Alex. Note that the single fluorescent label brightness, ϵ, is less than half of its value at high dilution (see Fig. 3), while the $S_{\sigma m}$ parameter, estimated from the first two points, stays consistent.

A physically different situation occurs at high surface densities of fluorescently labeled SAv, as shown in Fig. 4 for a layer containing 100% SAv-Alex. This curve exhibits a dramatic brightness recovery after an initial decay. By fitting the first part of the brightness variation, which is assumed to be linear, we estimated the $S_{\sigma m}$ parameter at 0.96, which is reasonably close to the value measured at 1% dilution. Conversely, the single fluorescent label brightness,

$\epsilon = 4.6$ kHz, is found to be less than half of the value measured at high dilutions of SAv-Alex (see Fig. 3). We suggest that fluorescence quenching between identical fluorophores can explain this behavior: at 100% concentration, the mean distance between the Alexa555 dyes is on the order of the size of the SAv molecules, which is ≈ 5 nm. At such short distances, the reduction in fluorescence quantum yield can be very pronounced.[18] When photobleaching occurs, the mean distance between intact fluorescent labels increases, thereby reducing self-quenching such that the brightness tends toward its normal value. Because this aspect is not within the scope of the present work, we did not study the exact shape of the brightness curve further, but we tentatively made use of the 100% concentration results to estimate the surface density of SAv. Using the waist size found for this 100% SAv-Alex case, $w_r = 0.25\mu m$ and $m = 1.7$ (middle of the range corresponding to $S_{\sigma m} = 0.96$), we estimate a surface density of 30,330 SAv molecules per μm^2. This number is close to 100 times the surface density measured at 1% dilution. Moreover, this value corresponds to a mean distance of 5.7 nm between SAv molecules, which is consistent with the assumption of a densely packed layer, given the size of a SAv molecule.[19] Therefore, although based solely on the first two points, the results obtained for 100% fluorescently labeled SAv are compatible with the lower-density case. Experiments have also been performed with 10% and 50% dilutions, the results of which are reported and synthesized in Table 1. Overall, our SAv-Alex results are consistent with each other, with a clear trend toward more fluorescent quenching as the surface density of SAv-Alex increases.

SAv has the same fluorescent label distribution on surfaces and in solution

To obtain an independent estimation of the fluorescent label distribution, we also applied our method to SAv-Alex molecules freely diffusing in solution. We found a value of $S_{\sigma m}$ that is highly consistent with the estimations on surfaces (approximately 0.8), as illustrated in Fig. 5A. As a control case, Fig. 5B shows that sulforhodamine B sodium salt (SRB) solutions

lead to a constant brightness under photobleaching, as expected for a single dye molecule.

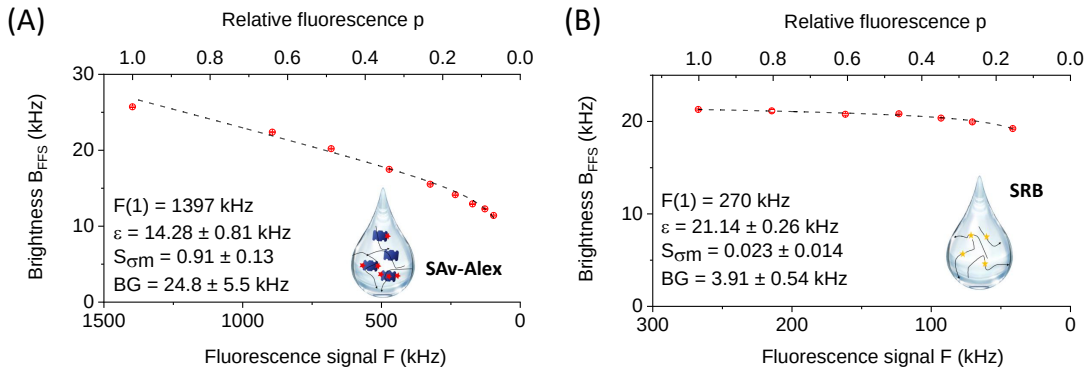

Figure 5: Examples of brightness decays measured by FCS for solutions confined in PDMS microwells. (A) SAv-Alex molecules, where the normalized slope, $S_{\sigma m}$, is close to the value found on surfaces (see Fig. 3). (B) SRB in HEPES, showing an almost constant brightness, in agreement with the expected behavior of a single dye molecule. For both cases, a background of up to 2% is estimated. Note that the error bars are smaller than the point size.

Biotinylated molecules bind to approximately 10% of the SAv molecules in the base layer

Next, we investigated the surface density of biotinylated molecules deposited on top of SAv layers, in order to show the potential of pbFFS as a characterization tool for developing biomimetic surfaces. Fluorescent bAtto molecules bound on a SAv base layer were observed. The brightness decay, as shown in Fig. 6A, exhibits a normalized slope, $S_{\sigma m} = 0.21$, which is significantly smaller than the slope observed for a SAv-Alex layer. This result indicates that this case is close to that of a single fluorescent label per labeled SAv molecule. Assuming the same type of distribution (i.e., over 1, 2, or 3 fluorescent labels), the range of m values corresponding to $S_{\sigma m} = 0.21$ is estimated as $[1.08, 1.12]$ (see Fig. S1 and Eq. S14 in the SI). Two quantities can be estimated from these measurements: the surface density of bAtto molecules given by $F(1)/\epsilon\pi {w_r}^2$, which is 3,708 molecules per μm^2, and the density of *fluorescently labeled* SAv molecules given by $F(1)/(m\epsilon\pi {w_r}^2)$ with $m = 1.1$, the center of the range estimated above, which is approximately $3{,}370/\mu m^2$. Because we previously found

$\sim$30,330 SAv molecules per μm^2 in the base layer, this result implies that approximately 1 in 10 SAv molecules carry at least a bAtto molecule. Note that the areal mass density reported in Table 1 is that of bAtto molecules.

Each SAv molecule has 4 biotin-binding sites: at least 1 of these sites is used to bind to the PLL-g-PEGbiotin base layer. Thus, the *a priori* number of available sites for bAtto is between 0 and 3. Our data indicate that 9 in 10 SAv molecules could not bind any bAtto, presumably due to steric hindrance. Concerning the fraction of labeled SAv, we furthered our analysis by using Eq. S12 in the SI with $m \sim 1.1$ and $S_{\sigma m} = 0.21$ and deduced that, *among the fluorescently labeled* SAv, approximately 90% of SAv bound only one bAtto, leaving 10% that carried more than one bAtto. Two mechanisms can lead to this distribution: either bAtto binds to SAv as single molecules, in which case a few SAv molecules have more than one occupied biotin-binding pocket, or bAtto pre-exists as dimers, trimers, etc. in the solution used for incubation, in which case, SAv may present only one pocket occupied by a bAtto complex.

To assess the relative effects of these two scenarios, we performed pbFFS experiments with bAtto solutions (FCS), as reported in the next section. Indeed, the fact that Atto dyes are moderately hydrophilic could favor aggregation.[20]

Biotinylated molecules show slight aggregation in solution

In Fig. 6B, we show an example of a photobleaching experiment with bAtto in solution. Globally, we recovered normalized slope values close to those found on a surface (i.e., $S_{\sigma m} \approx 0.2-0.3$), which are clearly distinct from the single-molecule case of SRB in solution, as shown in Fig. 5B. This range of $S_{\sigma m}$ values corresponds (see Fig. S1 in the SI) to a mean number of 1-1.2 fluorescent labels per diffusing entity for m, as summarized in Table 1. Because one bAtto molecule definitively corresponds to a single Atto dye molecule, we conclude that unspecific aggregation occurs between bAtto molecules in solution, despite the moderate concentration ($< \mu$M). Consequently, although the concentrations used to incubate the SAv

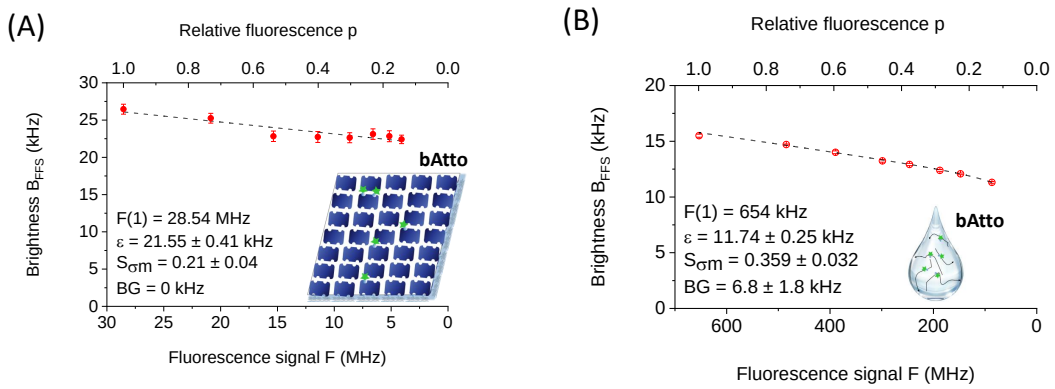

Figure 6: Brightness decay of biotinylated fluorescent molecules (bAtto), measured on a surface and in solution. (A) ICS measurements for bAtto bound to a SAv base layer, exemplifying the lower normalized slope value, $S_{\sigma m} = 0.21$, compared with SAv-Alex (the photophysical properties of these dyes cause bAtto to exhibit a single fluorescent label brightness different from that of Alexa555-labeled SAv). (B) FCS measurements for bAtto freely diffusing in solution. Note that the error bars are smaller than the point size.

base layer with bAtto are much lower than those used for FCS experiments (which should mitigate the aggregation trend), we cannot exclude the possibility that each SAv has only one bAtto binding site occupied by an aggregate. In this case, the number of available biotin-binding sites on the SAv layer is not the number of bound bAtto molecules (i.e., 3,708 / μm^2) but rather the number of SAv molecules labeled with bAtto (i.e., 3,370 / μm^2).

Note that the difference in brightness between bAtto in solution and on a SAv layer, as shown in Fig. 6, is not relevant, as the ICS and FCS experiments were performed on a surface and in bulk, respectively (with different microscopy setups). The same remark stands for the SAv results shown in Fig. 5A and Fig. 3.

pbFFS results agree with spectroscopic ellipsometry

In Table 1, we present the degree of fluorescent labeling (m) corresponding to different molecules, including SAv-Alex, bAtto, and SRB, in solution and on a surface. For each case, the lower and upper values of the m ranges estimated for the different experiments were pooled together to give a mean and SD for m. When applicable, these values were then used to derive the areal mass density of the SAv molecules. Although the photobleaching

Table 1: Degree of fluorescent labeling (m values) and areal mass density (when applicable) measured with pbFFS for different molecules on a surface and in solution. For SAv-Alex molecules diluted at 50%, 10%, and 1%, the estimated areal mass density is linearly extrapolated to 100% SAv. Values are given as the mean ± SD.

Molecule	**Sample**	**Fluo. Label.**	**Density (ng/cm^2)**
SAv-Alex	Surface 100%	1.79 ± 0.39	239 ± 34
SAv-Alex	Surface 50%	1.22 ± 0.05	303 ± 50
SAv-Alex	Surface 10%	1.94 ± 0.22	293 ± 69
SAv-Alex	Surface 1%	1.74 ± 0.36	284 ± 70
SAv-Alex	Solution	1.58 ± 0.18	n/a
bAtto	Surface	1.13 ± 0.09	0.82 ± 0.23
bAtto	Solution	1.125 ± 0.057	n/a
SRB	Solution	1.013 ± 0.011	n/a

decay curves of 100% SAv-Alex have a limited number of exploitable points (due to the above-mentioned quenching effect), the corresponding pbFFS estimation of the density is in fairly good agreement with the spectroscopic ellipsometry result, which gives 246 ± 36 ng/cm^2.[21] The linear extrapolation to 100% SAv for SAv-Alex molecules diluted at 1%, 10%, and 50% tends to show a higher areal mass density, but this effect may be related to the uncertainty of dilution. We also stress that although the degree of labeling found for 50% dilution differs from the other cases, the corresponding areal mass density is consistent with the other results.

Concerning bAtto, the reported areal mass density of 0.82 ± 0.23 ng/cm^2 corresponds to the total number of bAtto molecules bound to the SAv base layer. This value holds regardless of the bAtto distribution on the SAv molecules. Note that such low densities cannot be measured by ellipsometry; thus, no comparison can be made.

Discussion

We have presented a method, named pbFFS, which aims to estimate the number density of fluorescing entities. We have shown the potential of this method for reliable quantification in the context of biomimetic layer characterization, by comparing it with spectroscopic el-

lipsometry, a conventional quantitative method for studying surfaces. However, the latter technique requires dedicated substrates, while our technique can be performed on standard 96-well plates. Finally, unlike typical fluorescence-based techniques, pbFFS does not rely on a calibration process or homogeneous fluorescence labeling. Hereafter, we discuss two limiting situations.

In this work, we have measured surface densities spanning two orders of magnitude, from $\sim$300 to $\sim$30000 molecules per μm^2. The latter value is most likely close to the highest density that can be measured using ICS. Indeed, for a high concentration or density of molecules, the relative intensity fluctuations and, thus, autocorrelation amplitudes are very small and may be hidden by unwanted variations (non-uniformity in the imaging system or sample). Therefore, it is important to properly flatten images, to verify the stability of samples, etc. High densities can also induce detrimental photophysical effects, such as quenching. However, we experimentally showed that these effects do not prevent us from obtaining accurate results, provided that the biased data points are removed during analysis.

The SAv molecules studied here were labeled by 1-3 fluorophores, and thus, the degree of fluorescent labeling was rather low. One may wonder whether pbFFS would also be suitable for studying entities with a higher degree of fluorescent labeling (several tens of fluorophores or more). In this case, the photobleaching process starts with entities that are initially very bright and must be continued until only single fluorescent labels are left, which requires a high dynamic range of detection. Using fluorescent nanospheres, we verified that our framework applies to such situations in principle, as shown in Section S3 in the SI.

In addition to number density quantification, some applications may benefit from the ability of pbFFS to provide information on the degree of fluorescent labeling (or the number of fluorophores per entity), for example, as in oligomerization studies. Oligomerization is a ubiquitous phenomenon that plays an important role in numerous biological processes. The size of oligomers is usually estimated via fluorescence fluctuation methods (FCS, ICS) by a comparison between the measured brightness and the brightness of a sample containing

only monomers under the same experimental conditions. Such methods suffer from two drawbacks. First, a reference sample with only monomers may not be easily available. Second, if the oligomers do not all have the same size, the result is biased, resulting in an overestimation of oligomer size. More advanced techniques have been proposed, such as SpIDA,[22] FIF,[23] and eN&B,[24] but these methods still rely on the monomer brightness. The pbFFS method does not require a separate measurement of monomers, as the monomer brightness (ϵ) is provided by the fit. Thus, this approach is *self-calibrated*, which provides a significant advantage. Moreover, some information on the distribution of oligomer size can be obtained, although, as shown in this work, the exact distribution can only be resolved if the number of degrees of freedom is reduced by additional assumptions (*e.g.,* only few possible oligomers). This strategy would be suitable not only for fixed samples, but also for living cells. Photobleaching in live cells has been proposed, outside of the oligomerization context, to retrieve molecular brightness and to transform confocal images into concentration maps.[25] However, this method cannot be used for cases in which the studied protein forms homo-oligomers, in contrast to the present work.

Finally, although our method contrasts with standard semi-quantitative fluorescence approaches that cannot handle a brightness distribution, it can be compared with some single-molecules techniques based on stepwise photobleaching.[6,26,27] For instance, Madl et al. combined photobleaching and brightness analysis to measure the subunit composition of membrane proteins.[28] In a recent work, Stein et al. combined FCS with single-molecule localization microscopy to provide the number of docking strands in spatially well-separated origami nanostructures.[29] However, single-molecule techniques obviously require extremely low surface densities of immobilized molecules, while pbFFS works in much higher-density regimes, which are more relevant for most biomimetic and biological samples.

Conclusion

In this paper, we have presented a method that combines fluctuation analysis and photobleaching to characterize molecules or particles fluorescently labeled with an unknown distribution of fluorophores. pbFFS can be used both on a surface or in bulk, with immobilized or moving molecules (either flowing or freely diffusing), observed in confocal or total internal reflection fluorescence microscopy performed in photon counting mode. This method provides the single fluorescent label brightness, as well as a parameter depending on the mean and variance of the distribution of fluorescent labels. If additional assumptions can be used to restrict the number of degrees of freedom of this distribution, the degree of fluorescent labeling and an unbiased value of the concentration or density can be deduced.

The pbFFS method has been demonstrated on a SAv base layer of biomimetic samples to estimate the surface density of SAv and its propensity to bind a top layer of bAtto molecules. The base layer density estimated with pbFFS agrees well with ellipsometry measurements. However, compared with this latter technique or QCM-D, pbFFS has the advantage of allowing *in situ* characterization, as it does not require dedicated substrates. This method also enables the quantification of adsorbed molecules at low masses (as in the case of bAtto), which is beyond the capacity of the other techniques, due to the intrinsic sensitivity of fluorescence measurements.

We believe that pbFFS can provide a powerful framework for performing reliable fluorescence fluctuation analyses: indeed, with standard FFS techniques, it is not possible to assess whether the results are biased by a dispersion of brightness values (or number of fluorescent labels). In contrast, using pbFFS, the linear decay of the brightness during photobleaching is a simple checkpoint, which renders the measurements more trustworthy.

In addition to number density estimations, the capability to evaluate the number of fluorophores per entity makes pbFFS particularly useful for oligomerization studies, as estimating protein oligomerization is essential for elucidating numerous cellular functions.

Acknowledgement

We acknowledge D. Centanni (LIPhy) for the microwell preparation and the IAB facility for use of their confocal microscope. We thank M. Balland (LIPhy) and O. Destaing, A. Grichine (IAB) for stimulating discussions. We acknowledge E. Castro Ramirez for her work with PLL-g-PEGb. This project was funded by ANR GlyCON ANR-19-CE13-0031-01.

Supporting Information Available

Section S1 - Theoretical derivation of the brightness decay and exploitation of the measurements; Section S2 - Theoretical derivation of occupancy probabilities and m value ranges; Section S3 - Results and analysis of experiments with 20-nm fluorescent beads; Section S4 - Materials and methods (PDF).

References

(1) Martino, M. M.; Briquez, P. S.; Maruyama, K.; Hubbell, J. A. Extracellular matrix-inspired growth factor delivery systems for bone regeneration. *Adv Drug Deliver Rev* **2015**, *94*, 41–52.

(2) Migliorini, E.; Guevara-Garcia, A.; Albiges-Rizo, C.; Picart, C. Learning from BMPs and their biophysical extracellular matrix microenvironment for biomaterial design. *Bone* **2020**, *141*, 115540.

(3) Sefkow-Werner, J.; Machillot, P.; Sales, A.; Castro-Ramirez, E.; Degardin, M.; Boturyn, D.; Cavalcanti-Adam, E. A.; Albiges-Rizo, C.; Picart, C.; Migliorini, E. Heparan sulfate co-immobilized with cRGD ligands and BMP2 on biomimetic platforms promotes BMP2-mediated osteogenic differentiation. *Acta Biomater.* **2020**, *114*, 90–103.

(4) Migliorini, E.; Weidenhaupt, M.; Picart, C. Practical guide to characterize biomolecule adsorption on solid surfaces (Review). *Biointerphases* **2018**, *13*, 06D303.

(5) Waters, J. C.; Wittmann, T. *Methods Cell Biol.*; Elsevier, 2014; pp 1–18.

(6) Verdaasdonk, J. S.; Lawrimore, J.; Bloom, K. *Methods Cell Biol.*; Elsevier, 2014; pp 347–365.

(7) Slaughter, B. D.; Li, R. Toward Quantitative "In Vivo Biochemistry" with Fluorescence Fluctuation Spectroscopy. *Mol. Biol. Cell* **2010**, *21*, 4306–4311.

(8) Hennen, J.; Saunders, C. A.; Mueller, J. D.; Luxton, G. W. G. Fluorescence fluctuation spectroscopy reveals differential SUN protein oligomerization in living cells. *Mol. Biol. Cell* **2018**, *29*, 1003–1011.

(9) Kolin, D. L.; Wiseman, P. W. Advances in Image Correlation Spectroscopy: Measuring Number Densities, Aggregation States, and Dynamics of Fluorescently labeled Macromolecules in Cells. *Cell Biochem. Biophys.* **2007**, *49*, 141–164.

(10) Kitamura, A.; Kinjo, M. State of the Art Fluorescence Fluctuation Based Spectroscopic Techniques for the Study of Protein Aggregation. *Int J Mol Sci* **2018**, *19*, 964.

(11) Müller, J. D. Cumulant Analysis in Fluorescence Fluctuation Spectroscopy. *Biophys. J.* **2004**, *86*, 3981–3992.

(12) Delon, A.; Wang, I.; Lambert, E.; Mache, S.; Mache, R.; Derouard, J.; Motto-Ros, V.; Galland, R. Measuring, in Solution, Multiple-Fluorophore Labeling by Combining Fluorescence Correlation Spectroscopy and Photobleaching. *J. Phys. Chem. B* **2010**, *114*, 2988–2996.

(13) Ciccotosto, G. D.; Kozer, N.; Chow, T. T. Y.; Chon, J. W. M.; Clayton, A. H. A. Aggregation Distributions on Cells Determined by Photobleaching Image Correlation Spectroscopy. *Biophys. J.* **2013**, *104*, 1056–1064.

(14) Paviolo, C.; Chon, J. W. M.; Clayton, A. H. A. In *Biochemical and Biophysical Roles of Cell Surface Molecules*; Chattopadhyay, K., Basu, S. C., Eds.; Springer Singapore: Singapore, 2018; pp 41–52.

(15) Mets, R. D.; Wang, I.; Gallagher, J.; Destaing, O.; Balland, M.; Delon, A. Determination of protein concentration on substrates using fluorescence fluctuation microscopy. *Proc.SPIE* **2014**, *8950*.

(16) Dundas, C. M.; Demonte, D.; Park, S. Streptavidin–biotin technology: improvements and innovations in chemical and biological applications. *Appl. Microbiol. Biotechnol.* **2013**, *97*, 9343–9353.

(17) Brock, R.; Hink, M. A.; Jovin, T. M. Fluorescence Correlation Microscopy of Cells in the Presence of Autofluorescence. *Biophys. J.* **1998**, *75*, 2547–2557.

(18) Bae, W.; Yoon, T.-Y.; Jeong, C. Direct evaluation of self-quenching behavior of fluorophores at high concentrations using an evanescent field. *PLOS ONE* **2021**, *16*, e0247326.

(19) Hendrickson, W. A.; Pahler, A.; Smith, J. L.; Satow, Y.; Merritt, E. A.; Phizackerley, R. P. Crystal structure of core streptavidin determined from multiwavelength anomalous diffraction of synchrotron radiation. *Proc. Natl. Acad. Sci.* **1989**, *86*, 2190–2194.

(20) Zanetti-Domingues, L. C.; Tynan, C. J.; Rolfe, D. J.; Clarke, D. T.; Martin-Fernandez, M. Hydrophobic Fluorescent Probes Introduce Artifacts into Single Molecule Tracking Experiments Due to Non-Specific Binding. *PLoS ONE* **2013**, *8*, e74200.

(21) Migliorini, E.; Sefkow-Werner, J.; Licitra, C. Spectroscopic ellipsometry characterisation of Streptavidin Alexa binding to PLL-g-PEGbiotin(50%). Mendeley Data, V1, 2021; DOI:10.17632/kmshdrrs6y.1.

(22) Godin, A. G.; Rappaz, B.; Potvin-Trottier, L.; Kennedy, T. E.; Koninck, Y. D.; Wiseman, P. W. Spatial Intensity Distribution Analysis Reveals Abnormal Oligomerization of Proteins in Single Cells. *Biophys. J.* **2015**, *109*, 710–721.

(23) Stoneman, M. R.; Biener, G.; Ward, R. J.; Pediani, J. D.; Badu, D.; Eis, A.; Popa, I.; Milligan, G.; Raicu, V. A general method to quantify ligand-driven oligomerization from fluorescence-based images. *Nat. Methods* **2019**, *16*, 493–496.

(24) Cutrale, F.; Rodriguez, D.; Hortigüela, V.; Chiu, C.-L.; Otterstrom, J.; Mieruszynski, S.; Seriola, A.; Larrañaga, E.; Raya, A.; Lakadamyali, M.; Fraser, S. E.; Martinez, E.; Ojosnegros, S. Using enhanced number and brightness to measure protein oligomerization dynamics in live cells. *Nat. Protoc.* **2019**, *14*, 616–638.

(25) Zhang, L.; Perez-Romero, C.; Dostatni, N.; Fradin, C. Using FCS to accurately measure protein concentration in the presence of noise and photobleaching. *Biophys. J.* **2021**, *120*, 4230–4241.

(26) Wang, X.; Li, X.; Deng, X.; Luu, D.-T.; Maurel, C.; Lin, J. Single-molecule fluorescence imaging to quantify membrane protein dynamics and oligomerization in living plant cells. *Nat. Protoc.* **2015**, *10*, 2054–2063.

(27) Bryan IV, J. S.; Sgouralis, I.; Pressé, S. Diffraction-limited molecular cluster quantification with Bayesian nonparametrics. *Nat. Comput. Sci.* **2022**, *2*, 102–111.

(28) Madl, J.; Weghuber, J.; Fritsch, R.; Derler, I.; Fahrner, M.; Frischauf, I.; Lackner, B.; Romanin, C.; Schütz, G. J. Resting State Orai1 Diffuses as Homotetramer in the Plasma Membrane of Live Mammalian Cells. *J. Biol. Chem.* **2010**, *285*, 41135–41142.

(29) Stein, J.; Stehr, F.; Schueler, P.; Blumhardt, P.; Schueder, F.; Mücksch, J.; Jungmann, R.; Schwille, P. Toward Absolute Molecular Numbers in DNA-PAINT. *Nano Lett.* **2019**, *19*, 8182–8190.

TOC Graphic

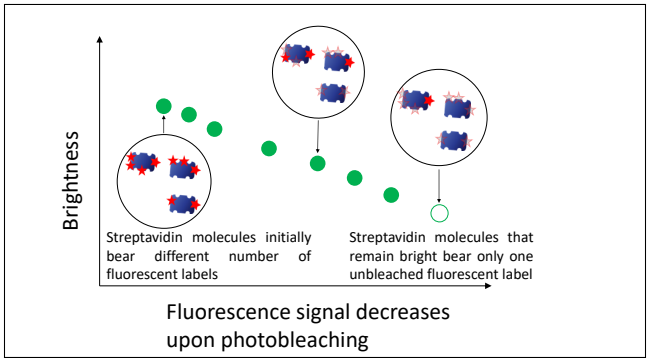
Brightness
Streptavidin molecules initially bear different number of fluorescent labels
Streptavidin molecules that remain bright bear only one unbleached fluorescent label
Fluorescence signal decreases upon photobleaching

Supporting Information: Combining fluorescence fluctuations and photobleaching to quantify surface density

Julius Sefkow-Werner,[†,‡] Elisa Migliorini,[*,†,‡] Catherine Picart,[†,‡] Dwiria Wahyuni,[¶,§] Irène Wang,[¶] and Antoine Delon[*,¶]

† *Univ. Grenoble Alpes, INSERM U1292, CEA, CNRS EMR 5000 BRM, IRIG Institute, CEA, 38054 Grenoble, France*

‡ *Grenoble Institute of Engineering, CNRS UMR 5628, LMGP, 38016 Grenoble, France*

¶ *Univ. Grenoble Alpes, CNRS, LIPhy, 38000 Grenoble, France*

§ *Current address: Department of Physics, Universitas Tanjungpura, Pontianak 78124, Indonesia*

E-mail: elisa.migliorini@cea.fr; antoine.delon@univ-grenoble-alpes.fr

Summary: Theoretical derivation of the brightness decay and exploitation of the measurements (S1); Theoretical derivation of occupancy probabilities and m value ranges (S2); Results and analysis of experiments with 20 nm fluorescent beads (S3); Materials and methods (S4).

S1. Theoretical derivation of the brightness decay and exploitation of the measurements

Theoretical derivation of the brightness decay

In the following, we derive the rigorous expression of the brightness B_{FFS} as a function of the photobleaching stage (defined as the fraction of remaining fluorescence signal), assuming all fluorophores are independent and have an equal probability to bleach. Although we present the formalism of pbFFS for two-dimensional ICS, the same results apply to mobile molecules and temporal techniques, *e.g.* FCS in solution, Raster ICS,[1] etc.

Let us consider $I(x, y)$ the image intensity at pixel x, y. The fluorescence fluctuations, defined as $\delta I(x, y) = I(x, y) - \langle I(x, y)\rangle$ (where the averaging is performed over the image field), are analyzed using the autocorrelation function:

$$G(\xi, \eta) = \frac{\langle \delta I(x, y)\delta I(x + \xi, y + \eta)\rangle}{\langle I(x, y)\rangle^2} \tag{S1}$$

In spatial ICS, the fluorescent entities of interest are immobile, so that the autocorrelation is only related to the optical resolution of the microscope (described by the PSF) and is very well approximated by a Gaussian:[2]

$$G(\xi, \eta) = \frac{1}{N_{FFS}} \exp\left(-\frac{\xi^2 + \eta^2}{w_r^2}\right) \tag{S2}$$

where N_{FFS} is an apparent mean number of entities in the PSF area of radius w_r. As already pointed out in the Introduction of the primary manuscript (Eq. 1), when the observed species are not equally bright, N_{FFS} is smaller than N, the real number of all the entities. In the case of a mixture of species of different brightness, it can be shown that the FFS techniques leads to:[1,3]

$$N_{FFS} = \frac{(\sum \epsilon_i N_i)^2}{\sum \epsilon_i^2 N_i} \tag{S3}$$

where ϵ_i is the brightness of the species i (that is the fluorescence signal of a single entity of the species i) and N_i, the average number of entities of the species i. Note that the true total number of entities is given by $N = \sum N_i$. The key point is that the contributions are weighted by the square of the brightness, leading to an underestimation of the total number of fluorescent entities, when all entities are not equally bright (it's the tree that hides the forest).

Here, we consider that each entity carries several identical fluorescent labels. In the forthcoming derivation we shall assume that fluorescence quenching can be neglected, so that the brightness of a single fluorescent label is constant whatever their number in the entities. In this case, the brightness of an entity carrying n fluorescent labels is $\epsilon_n = n\epsilon$ where ϵ is the brightness of a single fluorescent label, and the fluorescence signal reads (N_n being the number of entities that bear exactly n fluorescent labels):

$$F = \sum n\epsilon N_n \tag{S4}$$

The overall brightness is thus given by:

$$B_{FFS} = \epsilon \frac{\sum n^2 N_n}{\sum n N_n} \tag{S5}$$

To describe the photobleaching effect, we present a derivation based on the same hypothesis as in the work by Ciccotosto *et al.*[4] However, we generalize the formalism in order to provide a simple theoretical expression of the brightness for any initial distribution of fluorescent labels. At a given point during photobleaching, we assume that any fluorophore has the same probability not to be bleached, given by p. This implies that the initial number of fluorescent labels, n, which appears in Eq. S4 and S5 has to be replaced by the mean number of unbleached labels, which is simply given by np. Therefore the remaining fluorescence signal reads:

$$F(p) = \epsilon \sum npN_n = \epsilon pmN \tag{S6}$$

where $m = \frac{1}{N}\sum nN_n$ is the average initial number of fluorescent labels per entity, computed over all fluorescent entities (this can be called *degree of fluorescent labelling*). Note that p is nothing but the fluorescence signal normalized to its initial value, before photobleaching has started, i.e. $p = F(p)/F(1)$. In order to also modify Eq. S5 and make it valid all along photobleaching, we need to replace n^2 by the second order moment of the distribution at the fluorescence stage p. Since any fluorescent label can only be in two states, bleached or unbleached with respective probabilities $(1-p)$ and p, this quantity results from the binomial distribution and equates $np(1-p)+n^2p^2$. As a consequence, Eq. S5 becomes:

$$B_{FFS}(p) = \epsilon\frac{\sum[np(1-p)+n^2p^2]N_n}{pmN} \tag{S7}$$

We see that the numerator of Eq. S7 reveals, in addition to the mean value, m, of the initial number of fluorescent labels per entity, the mean value of its square, $\frac{1}{N}\sum n^2N_n$ that can be written σ^2+m^2, where σ is the standard deviation of the initial number of fluorescent labels per entity. Consequently, after a few simplifications, Eq. S7 can be written again:

$$B_{FFS}(p) = \epsilon(1+S_{\sigma m}p) \tag{S8}$$

where

$$S_{\sigma m} = \sigma^2/m + m - 1 \tag{S9}$$

Hence the measured brightness B_{FFS} is an affine function of the photobleaching stage p: the single fluorescent label brightness ϵ is its intercept at $p = 0$ (note that this is an immediate output of pbFFS, obtained without any assumption) and $S_{\sigma m}$ is its slope normalized by the single fluorescent label brightness. Let us rewrite here the equation stating the initial fluorescence signal:

$$F(1) = \epsilon mN \tag{S10}$$

Eq. S8, S9 and S10 are the core relations around which all our reasoning is based. Note

that studying the variation of the number of entities, instead of the brightness, *versus* the fluorescence signal, would be completely equivalent, as B_{FFS} and N_{FFS} are related through $F = B_{FFS}N_{FFS}$ (we drop out the $_{FFS}$ subscript in F because the fluorescence signal is not biased by fluctuation measurements). We will mostly discuss the brightness because, in absence of background, it always decays as a straight line when plotted as a function of the fluorescence signal (whatever the initial distribution of fluorescent labels), which is quite convenient for visual inspection of the experimental results. At this stage, it is interesting to make a few remarks about the pbFFS approach.

- First, we emphasize the fact that the parameters σ and m appearing in Eq. S9 and S10 characterize the *initial* distribution of brightness. Of course this distribution varies during photobleaching (it can be shown that it always converges towards a Poisson one), but the slope, $S_{\sigma m}$, depends only on the initial distribution.

- Although $B_{FFS}(p)$ is an affine function of p whatever the initial brightness distribution, a very peculiar situation is that of a mixture of entities bearing either no fluorescent label, or exactly one. This leads to $\sigma^2 = m(1-m)$, hence $S_{\sigma m} = 0$ and the measured brightness, $B_{FFS}(p)$, is constantly equal to ϵ, independently of the photobleaching stage. Indeed, all visible entities can only have the brightness of single labels.

- Another notable case is an ensemble of entities that initially bear the same number of labels, say an integer m (this is a single-valued distribution, with $\sigma = 0$). This would lead to a measured brightness, $B_{FFS}(p)$, that linearly varies from $m\epsilon$ to ϵ.

- In all cases, when the fluorescence signal vanishes ($p \to 0$), the measured brightness tends towards the one of a single label ($B_{FFS}(0) \to \epsilon$), since the only entities that remain visible are those bearing one single label. Consequently, one also obtains the total number of fluorophores that is just given by $mN = F(1)/\epsilon$.

- Finally, it is worth to notice that in case of an unknown proportion of dark entities,

there is obviously no way to assess it, and thus, to quantify the true total number of entities.

Exploitation of the measurements

Let us consider now what can be deduced from an experimental photobleaching decay, knowing that the measured normalized slope, $S_{\sigma m} = \sigma^2/m + m - 1$ and the intercept, ϵ, contain all the available information on the initial distribution of fluorescent labels from a pbFFS experiment. Therefore, in the general case, it is impossible to independently determine the mean value and the standard deviation of the number of fluorescent labels per entity. However, the values of these statistical parameters which are compatible with a given measured slope, $S_{\sigma m}$, can be represented by (σ, m) points located on a half circle of center $(0, \frac{1+S_{\sigma m}}{2})$ and radius $\frac{1+S_{\sigma m}}{2}$, as shown in Fig. S1. This half-circle can be seen as the support of the more general (σ, m) solution, independently of any specific kind of distribution.

The case of single-valued distributions (all entities bear the same *integer* number of fluorescent labels) corresponds to discrete points along the $\sigma = 0$ vertical axis. Another particular case is that of a Poisson distribution where the mean and the variance are related by $m = \sigma^2$, as depicted in Fig. S1. In this case, the photobleaching decay provides all necessary information to define the distribution. The measured brightness becomes $B_{FFS}(p) = \epsilon(1+mp)$, which is the same expression as the one obtained in Ref.,[5] but it is derived here in a more general framework. Note that, for small degrees of fluorescent labelling, the percentage of unlabelled species can be very large since, according to the properties of the Poisson distribution, it is given by e^{-m}.

In the general case where $S_{\sigma m} > 0$, the photobleaching slope can only provide a lower limit of the true number of entities N (and hence the surface density) but no upper bound: since $N = F(1)/m\epsilon$, the condition $m \leq 1 + S_{\sigma m}$ (see Fig. S1) leads to a lower bound, which equals the apparent value, $N_{FFS}(1) = F(1)/B_{FFS}(1)$, corresponding to the case where all entities have the brightness $B_{FFS}(1) = (1 + S_{\sigma m})\epsilon$. The fact that the real N cannot be lower

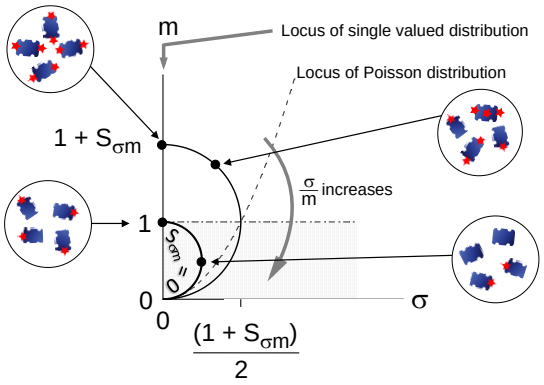

Figure S1: Geometrical representation of the relation between the mean, m, and the standard deviation, σ, of the *initial* number of fluorescent labels per entity. For a given measured slope, $S_{\sigma m}$, the support of the (σ, m) points is a half circle of diameter $1 + S_{\sigma m}$ that always crosses the $(0, 0)$ point; the coefficient of variation of the distribution of the number of fluorescent labels, $\frac{\sigma}{m}$, continuously increases from the top to the base of the half-circle. Single-valued distributions correspond to discrete points located on the vertical axis ($\sigma = 0$), as exemplified for 1 and 2 fluorescent labels. The smallest circle of diameter 1 ($S_{\sigma m} = 0$) corresponds to a mixture of entities bearing either no fluorescent label or exactly one, as depicted at the bottom right. If all molecules bear at least one fluorescent label, for instance a mixture of 1, 2 and 3 fluorescent labels, the (σ, m) solutions are located in the upper half space above the dashed-dotted line $m = 1$. Note that in the case of a Poisson distribution, any given slope $S_{\sigma m}$ corresponds to a unique point (σ, m) located at the intersection of the $m = \sigma^2$ curve (dashed line) and of the half circle of diameter $1 + S_{\sigma m}$ (see text).

than the apparent N_{FFS} is not new, since we argued that a distribution of brightness *always* causes FFS to underestimate the number of entities (see Eq. 1 in the primary manuscript). An upper bound for N can be established if we consider only *fluorescent* entities: in this case, the minimum value of m is larger than 1. Therefore, the true number of *fluorescent* entities is included between $N_{FFS}(1)$ and $F(1)/\epsilon = (1 + S_{\sigma m})N_{FFS}(1)$.

To summarize, the pbFFS method is useful if the initial fluorescent label distribution can be fully described by a limited number of degrees of freedom. When there is only one, the fluorescent label distribution can be estimated from the photobleaching slope, which makes it possible to determine the true number of entities. This is for instance the case for a Poisson law, as already used for DNA or fibrinogen fluorescent labelling.[5,6] Another example is that of a sample where all entities are uniformly fluorescently labelled. When the number

of degrees of freedom of the distribution is two, it may nevertheless be possible to infer a range of values for the number of entities, by combining the constraints of the fluorescent label distribution with the relation between σ and m as established by the measured slope. This is the case encountered in the current work with SAv molecules, which are assumed to bear 1, 2 or 3 fluorescent labels.

S2. Theoretical derivation of occupancy probabilities and m value ranges

When the number of fluorescent labels borne by an entity can only take 3 non-nil values, its distribution depends on 2 independent parameters, because of the normalization. This means that for a measured parameter $S_{\sigma m}$ (that equates $\sigma^2/m + m - 1$), any given possible value of m fully determines the 3 occupancy probabilities. The fact that these probabilities are to be between 0 and 1 implies limited ranges of values for m. We now exploit this simple mathematical framework in the particular case of 1, 2 and 3 fluorescent labels, but it can be easily extended to any distribution with 3 non-nil occupancy probabilities (more generally, when the distribution of the number of fluorescent labels depends on 2 independent parameters, whatever they are, this induces constraints on m that depend on the measured value of $S_{\sigma m}$).

Let us now consider the mean value, m, the standard deviation, σ and the normalisation of the distribution. These are given by:

$$\begin{aligned} m &= p_1 + 2p_2 + 3p_3 \\ \sigma^2 &= (1-m)^2 p_1 + (2-m)^2 p_2 + (3-m)^2 p_3 \\ p_1 + p_2 + p_3 &= 1 \end{aligned} \tag{S11}$$

where p_1, p_2 and p_3 are the probabilities to find 1, 2 and 3 fluorescent labels. These

equations can be easily transformed to express p_1, p_2 and p_3 as functions of m and σ:

$$\begin{aligned} p_1 &= 3 + m(S_{\sigma m}/2 - 2) \\ p_2 &= -3 + m(3 - S_{\sigma m}) \\ p_3 &= 1 + m(S_{\sigma m}/2 - 1) \end{aligned} \tag{S12}$$

By writing that each of these probability occupancies is between 0 and 1, one obtains the corresponding constraints on m as a function of $S_{\sigma m}$:

$$\begin{aligned} \frac{4}{4 - S_{\sigma m}} \leq m \leq \frac{6}{4 - S_{\sigma m}} \\ \frac{3}{3 - S_{\sigma m}} \leq m \leq \frac{4}{3 - S_{\sigma m}} \\ 0 \leq m \leq \frac{2}{2 - S_{\sigma m}} \end{aligned} \tag{S13}$$

We show in Fig. S2 the series of $m(S_{\sigma m})$ curves giving these upper and lower limits. Henceforth, the common region where all the constraints are simultaneously satisfied (hatched area) is defined by:

$$\frac{3}{3 - S_{\sigma m}} \leq m \leq \frac{2}{2 - S_{\sigma m}} \qquad \text{for} \qquad 0 \leq S_{\sigma m} \leq 1 \tag{S14}$$

$$\frac{3}{3 - S_{\sigma m}} \leq m \leq \frac{6}{4 - S_{\sigma m}} \qquad \text{for} \qquad 1 \leq S_{\sigma m} \leq 2 \tag{S15}$$

It is possible to add further restrictions regarding the distribution of the number of fluorescent labels. For instance, concerning the SAv-Alex molecules the specifications of which indicate an average of 2 fluorescent labels per molecule, it is reasonable to discard the cases where $p_3 > p_2$, which leads to $m > \frac{1}{1 - \frac{3}{8} S_{\sigma m}}$.

Finally, it is also interesting to ask what one would expect if one assumed that the entities

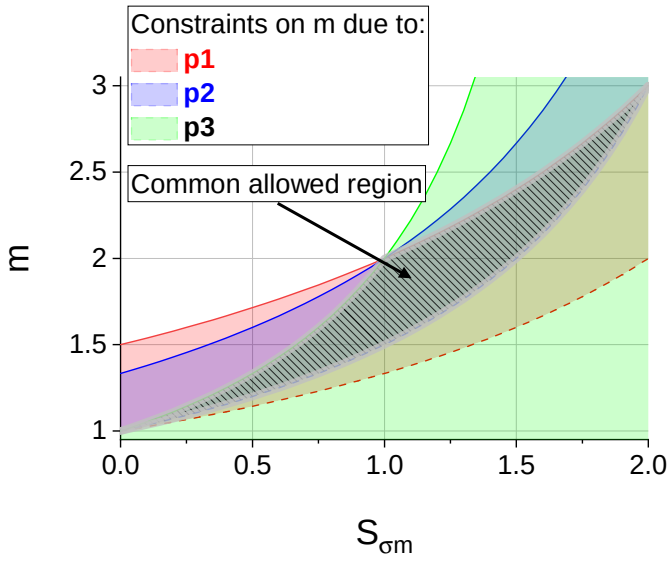

Figure S2: Limits of the possible values of m. For each value of $S_{\sigma m}$, the occupancy probabilities for 1, 2 and 3 fluorescent labels (p_1 (red zone), p_2 (blue) and p_3 (green)) are to be between 0 and 1, which implies corresponding minimum and maximum values of m. The common zone, allowed for any of the occupancy probabilities, is hatched and surrounded in gray.

could carry 2, 3 or 4 fluorescent labels. A derivation analogous to that leading to the above Eq. S11 to S13 gives:

$$\begin{aligned} \frac{8}{5-S_{\sigma m}} \leq m \leq \frac{9}{5-S_{\sigma m}} \\ \frac{10}{6-S_{\sigma m}} \leq m \leq \frac{12}{6-S_{\sigma m}} \\ \frac{4}{4-S_{\sigma m}} \leq m \leq \frac{6}{4-S_{\sigma m}} \end{aligned} \tag{S16}$$

S3. Experiments with 20 nm fluorescent beads

We performed experiments by plating 20 nm red fluorescent polystyrene beads (FluoSpheres™ Carboxylate Modified Microspheres, F8786, Invitrogen) on a glass substrate (Lab-Tek™II Chambered Coverglass, Nunc) that was previously treated with O_2 plasma, covered by poly(l-lysine) and then washed. After a few hours of incubation, the surface was rinsed with miliQ

water to remove unbound beads. 9 different zones of 25.7×25.7 μm^2 were imaged, using the same acquisition and analysis protocol as the one described in the main part of the manuscript.

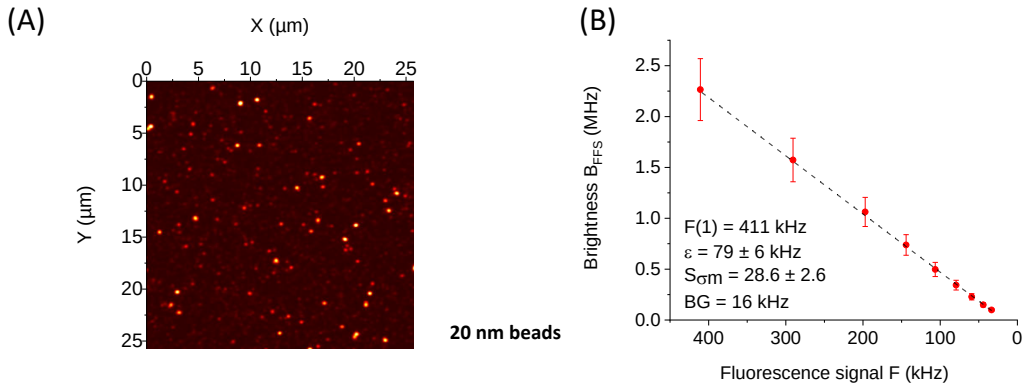

Figure S3: Analysis of 20 nm fluorescent beads deposited on a glass surface. (A) Initial image (before photobleaching) of one of the 9 zones (25.7×25.7 μm^2); (B) Corresponding brightness decay, the slope of which, $S_{\sigma m}$, is many tens of times larger than the one measured with SAv-Alex or bAtto molecules.

We see in Fig. S3A an image of one zone of beads and the corresponding photobleaching decay, the different zones showing the same trend. The striking property is the typical value of the slope, $S_{\sigma m}$, of a few tens (see Fig. S3B), that is much larger than the one obtained with SAv-Alex or bAtto molecules. Exploratory single particle detection, on images acquired at sufficiently low surface concentration, has confirmed that the bead intensity distribution is very broad, as one can guess according to Fig. S3A. Assuming that the distribution of the number of fluorescent labels follows a Poisson law, we can deduce that the mean number of fluorophores per bead is also of the order of a few tens (since in this case $m = S_{\sigma m}$), in agreement with the rough specifications given by the manufacturer.

We nevertheless stress the fact that the output parameters of the brightness decay fit might be very sensitive to the background. The reason relies in the very small final value of the brightness (that of the last measured point), relatively to the initial (unbleached) brightness. Depending upon the value found or fixed for the background, the estimated single fluorescent label brightness can vary a lot and so can the slope $S_{\sigma m}$.

Finally, these data show that pbFFS can in principle be applied to particles with a high degree of fluorescent labelling, although, to be reliable, measurements should be performed with a high dynamic range and a carefully controlled background.

S4. Materials and methods

Substrate preparation

Microscopy glass coverslips (24×24 mm, Menzel Gläser) were cleaned under sonication with acetone and isopropanol and blow-dried with nitrogen. They were UV/ozone activated (UV/Ozone ProCleaner Plus, Bioforce) for 10 min, attached to a microscopy support and PLL(20)-g[3.5]-PEG(2)/PEGbiotin(3.4)50% (≈107 kDa, SuSoS AG) was incubated at 10 μg/ml in 10 mM Hepes buffer (Fisher, pH=7.2) for 45 min.[7] Streptavidin (≈55kDa, Sigma Aldrich), SAv, and streptavidin Alexa Fluor™555 conjugate (≈55kDa, Molecular probes), SAv-Alex, with a labeling degree of 2 fluorophores (certificate of analysis, Molecular probes) were mixed in a ratio varying from 100:1 to 100:100 at 10 μg/ml in Hepes buffer and incubated for 30 min. A layer of biotinylated species was prepared by immobilizing Atto-labelled biotin (Atto 565-Biotin, 921 Da, Sigma-Aldrich), bAtto, to a saturated layer of SAv, bAtto occupying the free biotin pockets on SAv. In all cases, the sample was rinsed 5 times with Hepes after incubation.

Confocal imaging and photobleaching of surfaces

Functionalized glass coverslips were imaged using a Leica SP8 confocal microscope with a HC PL APO 63×1.2 water-immersed objective. The focal plane was determined where intensity was at maximum and then stabilized using the Adaptive Focus Control mode. The signal was detected with a hybrid detector working in the photon counting mode. An area of 25×25 μm^2 with 512×512 pixels was imaged 10 times with a pixel dwell time of 5 μs and a reduced laser intensity at 561 nm, so not to saturate and not to bleach the sample during

image acquisitions. Then, this area was photobleached with a sufficient illumination dose (scanning time×laser power) to loose roughly 30% of the initial signal and 10 images were acquired as before. This procedure was typically repeated 6 to 8 times, in order to finish the acquisition with a remaining signal of at most 10% of the initial one.

Image pre-processing and ICS

Before performing ICS analysis, it is necessary to correct the non-uniformity of the image intensity in the 1 - 10 μm scale range because, as already discussed in,[6] it can have a strong impact on the autocorrelation function. This non-uniformity originates, either from a spatial dependence of the light efficiency of the imaging system, or from an inhomogeneous surface density. It induces long range correlations that add to the autocorrelation of interest with various detrimental effects, such as anomalous base line, width and long range behaviour. Image flattening is especially crucial when the surface density is very high and thus the autocorrelation very weak, because in this case the relative bias can be very pronounced. In order to leave the ratio of the fluctuation amplitude to the mean value unchanged, on which the estimated number of entities depends, the images are flattened by dividing them by their own smoothed version. The latter is obtained by convoluting the original image with a two-dimensional Gaussian function. The width of this Gaussian has to be small enough to damp as much as possible image inhomogeneities, but significantly larger than the radius of the ICS PSF area ($w_r \approx 0.23\mu m$), in order not to bias the number fluctuations. Consistently with our previous study,[6] the $1/e$ half width of the Gaussian function used to smooth and flatten the images was chosen to be 2 μm. In practice, the images are individually flattened and autocorrelated. Then, for each photobleaching stage, the mean autocorrelation is fitted with Eq. S2 (see Supplementary Information), which gives a global estimation of N_{FFS} and the radius w_r. By verifying that the latter varies by much less than 1% during the acquisition process, we check the stability of the focus. The final goal being to analyze the variation of the brightness, B_{FFS}, *versus* the fluorescence signal F (i.e. the intensity), the images

are divided in 8×8 sub-images that are individually analyzed by ICS, while the value of the radius w_r is set at the one estimated from the whole image, thus providing a mean and a standard deviation of the mean of the brightness at each photobleaching stage. The image processing (flattening, autocorrelation and fit) was performed using Matlab (Mathworks).

Sample preparation and photobleaching of solutions

To achieve photobleaching of the fluorescent labels in solution in a reasonable amount of time (a few minutes), with the available laser power ($\leq$1 mW), the solutions were confined in poly(dimethylsiloxane) (PDMS) microwells. A regular array containing pillars of 100 μm in diameter and 100 μm in height with a pitch of 400 μm was fabricated on the Si wafer. After peeling off the mold, the 2 mm thick PDMS micropatterned slabs were activated with air plasma (Atto, Diener) for 2 min to achieve a hydrophilic surface.[5] Then a droplet of SAv-Alex or bAtto Hepes solution was placed on the PDMS block to enter the microwells, at initial concentrations around a few 100 nM. Such concentrations, relatively high for FCS, were necessary to saturate the microwell walls and avoid too much adsorption/desorption processes that induce unstable fluorescence signal. For control purposes, we also used solutions of Sulforhodamine B sodium salt, SRB (Sigma-Aldrich, St. Louis, USA), without further purification, diluted in either deionised water or Hepes. The PDMS block was flipped onto a Lab-Tek™Chambered Coverglass (Nunc) to seal the microwells and thus avoiding fluid exchange with the environment.

FCS acquisition and fit

The signal inside the microwells was acquired using a Nikon confocal microscope (Ti2E - A1R) with a 60×water-immersed objective and a reduced laser power at 561 nm, to avoid any photobleaching during FCS acquisitions. The latter were performed using a custom made detection system, comprising a 50/50 beam splitter and a pair of avalanche photodiodes (SPCM-AQRH-44-FC, EXCELITAS) to avoid after-pulsing effects, which was connected on

the auxiliary port of the microscope using a multimode optical fiber. The focal plane was set at 20 μm inside the microwells and photons were counted during 5 periods of 20 s to provide an averaged cross-correlation curve (and its corresponding standard error of the mean) using a Correlator.com software (Flex99r-12D). Proper optical adjustments and stability were controlled by fitting the diffusion time[8] and measuring the brightness of a reference dye, namely sulfo-rhodamine B. Each FCS acquisition thus gives an estimation of the number of entities, N_{FFS} and of the corresponding brightness, B_{FFS}, with a given uncertainty; it was followed by a bleaching cycle with a laser intensity adjusted to typically reduce the initial signal by 30% before performing the next acquisition. This was repeated 5 to 8 times until about less than 10% of the initial signal remains, in order to provide the variation of the brightness, B_{FFS}, with error bars, *versus* the fluorescence signal F (or photon count rate).

References

(1) Kolin, D. L.; Wiseman, P. W. Advances in Image Correlation Spectroscopy: Measuring Number Densities, Aggregation States, and Dynamics of Fluorescently labeled Macromolecules in Cells. *Cell Biochem. Biophys.* **2007**, *49*, 141–164.

(2) Petersen, N.; Höddelius, P.; Wiseman, P.; Seger, O.; Magnusson, K. Quantitation of membrane receptor distributions by image correlation spectroscopy: concept and application. *Biophys. J.* **1993**, *65*, 1135–1146.

(3) Müller, J. D. Cumulant Analysis in Fluorescence Fluctuation Spectroscopy. *Biophys. J.* **2004**, *86*, 3981–3992.

(4) Ciccotosto, G. D.; Kozer, N.; Chow, T. T. Y.; Chon, J. W. M.; Clayton, A. H. A. Aggregation Distributions on Cells Determined by Photobleaching Image Correlation Spectroscopy. *Biophys. J.* **2013**, *104*, 1056–1064.

(5) Delon, A.; Wang, I.; Lambert, E.; Mache, S.; Mache, R.; Derouard, J.; Motto-Ros, V.;

Galland, R. Measuring, in Solution, Multiple-Fluorophore Labeling by Combining Fluorescence Correlation Spectroscopy and Photobleaching. *J. Phys. Chem. B* **2010**, *114*, 2988–2996.

(6) Mets, R. D.; Wang, I.; Gallagher, J.; Destaing, O.; Balland, M.; Delon, A. Determination of protein concentration on substrates using fluorescence fluctuation microscopy. *Proc.SPIE* **2014**, *8950*.

(7) Huang, N.-P.; Vörös, J.; Paul, S. M. D.; Textor, M.; Spencer, N. D. Biotin-Derivatized Poly(l-lysine)-g-poly(ethylene glycol): A Novel Polymeric Interface for Bioaffinity Sensing. *Langmuir* **2002**, *18*, 220–230.

(8) Muller, P.; Schwille, P.; Weidemann, T. PyCorrFit–generic data evaluation for fluorescence correlation spectroscopy. *Bioinformatics* **2014**, *30*, 2532–2533.

TOC Graphic

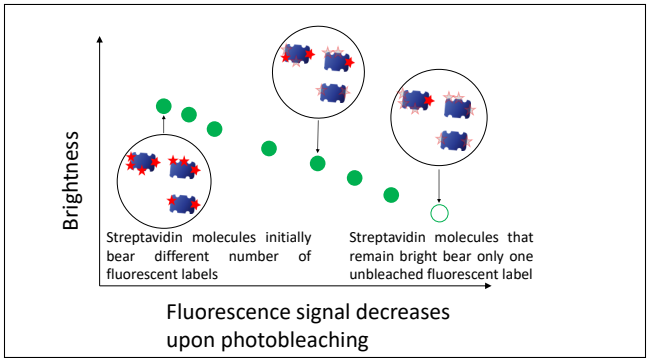
Brightness
Streptavidin molecules initially bear different number of fluorescent labels
Streptavidin molecules that remain bright bear only one unbleached fluorescent label
Fluorescence signal decreases upon photobleaching